Gabor domain analysis of Q in the nearsurface

Robert J. Ferguson, Gary F. Margrave, and Kevin W. Hall

SUMMARY

We present a Q estimation method based on traveltime derivatives applied to multilevel vertical seismic profile (VSP) acquisition. Long, narrowband vibroseis sweeps provide approximately monochromatic wavefields over short time windows, and analysis is done in the Gabor domain. There, attenuation β is estimated as a function of frequency f, and $Q(f)$ is computed through inversion of β.

We provide an example based on a 7-level, near-offset VSP. Each VSP level consists of a 3-component receiver with inline, crossline, and vertical sweeps. Eight, narrowband sweeps are used to span 10 Hz - 250 Hz for each source orientation, and they are found to help reduce noise in the data due to baseplate harmonics.

Two subunits are identified within the local formation that correspond to an expected 50 m of unsaturated media underlain by an aquifer. Our results demonstrate that β varies near-linearly with frequency for the 95 m depth range, Strong values of β that increase with f are found in the unsaturated unit, and weaker, decreasing β is found in the saturated unit.

Q for the formation is estimated only approximately due to excessive powerline noise and and strong harmonics in the well. For both units and the overall formation, Q increases linearly with f until about 100 Hz.

INTRODUCTION

Individual frequencies (f) within a propagating seismic wavefield are attenuated by most geological media Zener (1948). Quality factor Q_f is a common measure of this attenuation, and it is defined by

$$Q(f) = -\frac{2\pi E_f}{\Delta E_f}, \tag{1}$$

where, E is peak strain energy, and ΔE is energy loss per wave cycle (Zener, 1948). Q estimates are usually stationary in f, and they are determined through slope fitting amplitude spectra (spectral ratio method, Båth (1974)). In this approach, given two measurements of the same source waveform at two different points in space, the log of the ratio of their f spectra is used to estimate Q by slope fitting along the f coordinate. The result is a stationary estimate for Q; it is assumed to be constant for all f, and this is not consistent with the fundamental definition of Q (equation 1 above. Moreover, because slopes are fit along f, Q estimates are significantly impacted by noise sources.

As an alternative to the spectral ratio, we employ multi-level VSPs, and we fit slopes the log power spectra of these data along a time axis determined by raytracing. We require a good velocity profile which we have from a check-shot survey, and we obtain isolated, noise free f domain data at multiple levels through the Gabor transform (Sun et al., 2009).

The $Q(f)$ can be used as is, or an average Q can be computed that excludes f ranges thought to be contaminated by noise.

THEORY

Propagation of planewave G in a homogeneous attenuative medium is modelled by

$$G(\tau, f) = A(f)\ e^{-\beta(f)\,\tau}\, e^{i\,\phi(\tau,f)}, \tag{2}$$

where f is frequency in Hz, A is source amplitude, ϕ is phase in radians, τ is traveltime in seconds between source and receiver, and attenuation β (Hz) is given by

$$\beta(f) = \pi\, f/Q. \tag{3}$$

Quality factor Q (dimensionless) is characteristic of the effective attenuation of the medium between source and receiver (Jannsen et al., 1985). Equation 2 forms the basis for many Q estimation processes most notably the spectral ratio method (Båth, 1974). Phase ϕ describes the kinematics and dispersion of wave propagation and is of interest in seismic velocity inversion (Sun et al., 2009; Toverud and Ursin, 2005). Power $G\,G^{\dagger}$ of equation 2 eliminates the phase term according to

$$G(\tau, f)\ G(\tau, f)^{\dagger} = A^2(f)\ e^{-2\,\beta(f)\,\tau}, \tag{4}$$

and it returns a real valued, positive result. So, for $A > 0$,

$$\log\left\{\sqrt{G(\tau, f)\ G^{\dagger}(\tau, f)}\right\} = \log\{A(f)\} - \beta(f)\ \tau, \tag{5}$$

is a linear function with slope β. For a multidepth VSP, τ is traveltime from receiver level to receiver level, and $\beta(f)$ is obtained if we differentiate equation 5 along τ. Equations 3 and 5 suggest that if $\log\sqrt{G\,G^{\dagger}}$ by least-squares fit of equation 5 in τ we may estimate Q for all f. We assume here that Q is τ independent and we use formation by formation analysis to obtain $Q(\tau)$.

DATA ACQUISITION

To explore Q prediction based on equation 5, we acquired a 10 m offset VSP with a multilevel (7 levels spanning 10-95 m), 3-component downhole tool, a number of narrow frequency-band sweeps with sources in the vertical (V), inline horizontal (H_1), and crossline horizontal (H_2) directions. Note, for the V and H_1 sources, particle motion lies within the the plane that contains both the source and the wellbore; V is normal to the Earth's surface, and H_2 is parallel to that surface. H_2 particle motion is normal to the source-wellbore plane. A summary of sweeps and receiver depths is given in Tables 1 and 2 respectively. For each of the 7 depths, a multicomponent recording is made for each of tree sweeps for a total of 504 traces.

Simultaneous with the VSP data is a recording of 8 channels at the surface using vertical geophones for use as a reference array. This small array was located 10 m from the multicomponent the source with a trace spacing of 1 m.

Sweep (Hz)	1	2	3	4	5	6	7	8
V	10-250†	10-25	15-35	25-50	40-70†	60-105	95-155	145-250†
H_1	14-250†	14-25	15-35	25-50	40-70†	60-105†	95-155†	145-250†
H_2	14-250†	14-25	15-35	25-50	40-70†	60-105†	95-155†	145-250†

Table 1. Vibroseis sweeps for vertical (V), inline horizontal (H_1), and crossline horizontal (H_2). Daggers † indicate sweeps that vary in amplitude between receivers (see the section titled Data Acquisition) .

#	1	2	3	4	5	6	7
Depth (m)	95	90	80	70	55	30	10

Table 2. Depths to multi-component receivers 1-7.

Sources of noise

Analysis of the VSP data indicates a number of problems that include: source variation between downhole receivers, base-plate harmonics, electrical noise, plus a very-strong harmonic at $\sim$ 38 Hz. A number of missing sweeps (Tables 3 and 4) and a small number of erroneous sweeps (Table 5) are identified through simple, spectral analysis.

Source variation between downhole receivers

Q estimation according to equation 5 requires amplitude variation that is restricted to the attenuation mechanism, so all aspects of the survey must be constant. A difficulty arises, however, because of our use of a single level VSP tool. The 7 recorded levels (Table 2) are acquired one-at-a-time from the bottom of the well to the top. Source variability between downhole receivers, then, must be identified and corrected.

To assess source variation between downhole receivers, the graphs in Figure 1 are natural logarithms of the amplitude spectra of all traces recorded in the surface array (the array was live during the recording of each downhole receiver), and the various graphs are the result of grouping these log-spectra according to the range of the V sweep. Figure 1a, for example, corresponds to V sweep 10 - 250 Hz as indicated by the dashed blue lines. Figure 1b corresponds to V sweep 10 - 25 Hz and so on. Seven sweeps (Table 1), one for each depth (Table 2), are represented by three lines on each graph - a red line for the mean log-amplitude of the seven sweeps, and two black lines for the minimum and maximum log-amplitude of the 7 sweeps (one for each receiver depth) respectively. In Figure 1c, for example, the sweep range is 15 - 35 Hz and within that range, the mean (red), mini-

Depth (m)	Sweep (Hz)
30	15-35
50	145-250
70	145-250
90	14-25
95	40-70
95	145-250

Table 3. Missing vibroseis sweeps for inline horizontal (H_1).

Depth (m)	Sweep (Hz)
50	145-250
80	145-250
90	14-25

Table 4. Missing vibroseis sweeps for crossline horizontal (H_2).

Depth (m)	Sweep (Hz)	notes
90	145-250	$\sim$ 145-230
95	145-250	$\sim$ 145-230

Table 5. Messed up vibroseis sweeps for crossline horizontal (H_2).

mum(black), and maximum (black) values are the same. Beyond this design range, and in particular between 80 Hz and 250 Hz, red is visible though this is of no concern as long as data are interpreted only within the design range of the sweep.

V sources associated with sweeps (in Hz) of 10-250, 40-70, and 145-250 (Figures 1a, d, and h respectively) all have visible red lines in their log-amplitude spectra, so the source changes between receivers for these sweeps (indicated by daggers † in Table 1). V sources associated with sweeps (in Hz) of 10-25, 15-35, 25-50, and 95-155 Hz ((Figures 1b, c, e, and g respectively) have minimal variation. Similar analysis for sources H_1 and H_2 reveals well-to-well sweep variations in sweeps 14-250, 40-70, 60-105, 95-155, and 145-250 (the same for both sources), with minimal variation for sweeps 14-25, 15-35, and 25-50 (all in Hz).

Baseplate harmonics

Analysis of the uncorrelated surface data indicate that baseplate harmonics * are present on all sources. This can be seen in Figures 4, 5, and 6. In Figure 4, for example, the design sweep for source V is 25-50 as indicated by the dashed red line, and sweep energy does track this line as expected. (The live downhole receiver was at 95 m depth when this source was recorded). A second sweep is apparent, however, between 50 and 100 Hz for the entire sweep time; it is of lesser amplitude and opposite polarity. The indicated 38 Hz on Figure 4 (and Figures 6 and 6) corresponds to a harmonic that is considered later on in this paper.

Source H_1 for this 25-50 Hz sweep range (downhole tool at 9m m depth) indicates two strong baseplate-harmonics as can be seen in Figure 5. The frequency range of the first harmonic is the same as for the V source, but it is much stronger and of the same polarity as the fundamental sweep. The second harmonic between 75 and 120 Hz is weaker and of like polarity.

Source H_2 (Figure 6, 25-50 Hz, 95 m depth) has harmonics with similar amplitude and polarity behaviour as H_1 with higher amplitude concentrated at low frequency in the first harmonic.

*Vibrating systems consist of a fundamental and higher order (higher frequency) harmonics. For vibroseis, the fundamental is the design sweep, and the harmonics are higher frequency copies of the fundamental.

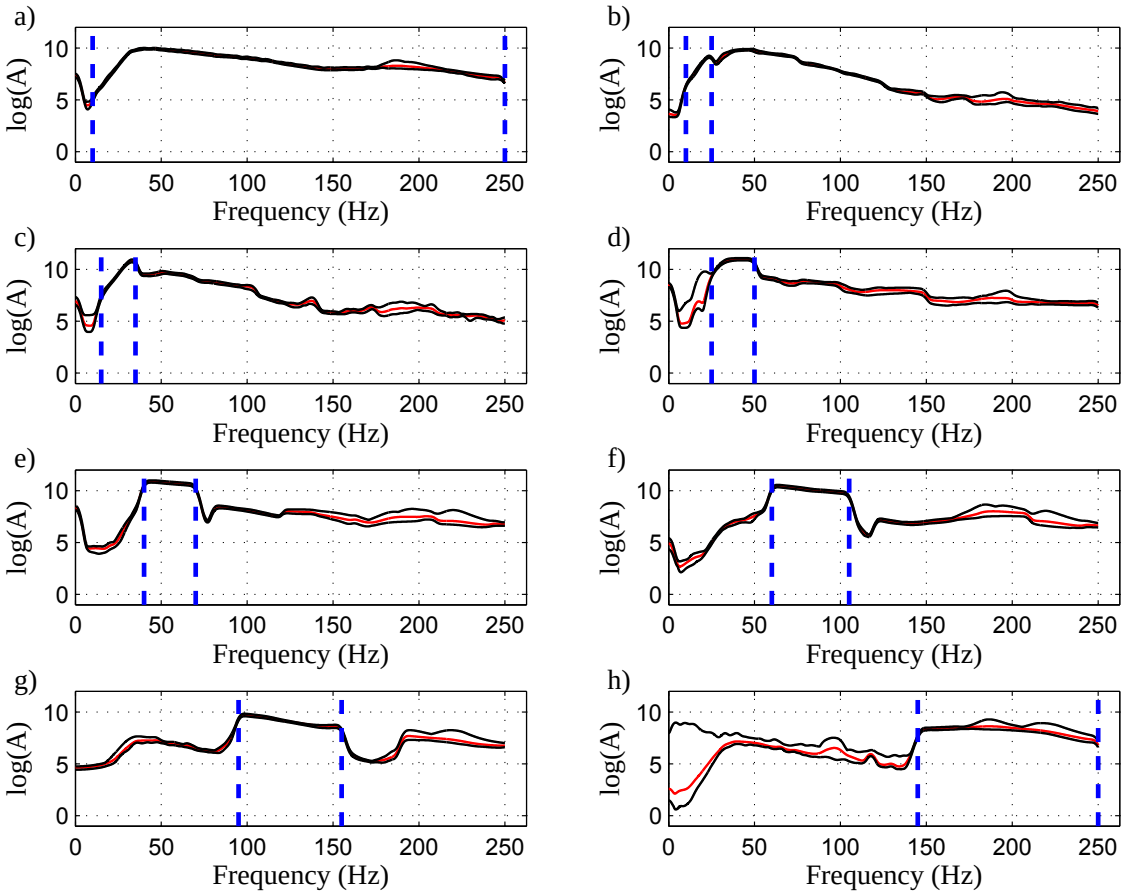

FIG. 1. Source V repeatability comparison. Sweep rangess in Hz are indicated by dashed black lines for 10-250 (a), 10-25 (b), 15-35 (c), 25-50 (d), 40-70 (e), 60-105 (f), 95-155 (g), and 145-250 (h) respectively. The red line is the mean value of $log(A)$ for all sweeps corresponding to depths 95, 90, 80, 70, 50, 30, and 10 m. Black lines correspond to the maxima and minima. Signif cant departure from the mean is seen outside of the target ranges of all sweeps, and signif cant departure is seen within the target ranges in Hz of 10-250 (a), 40-70 (d), and 145-250 (h).

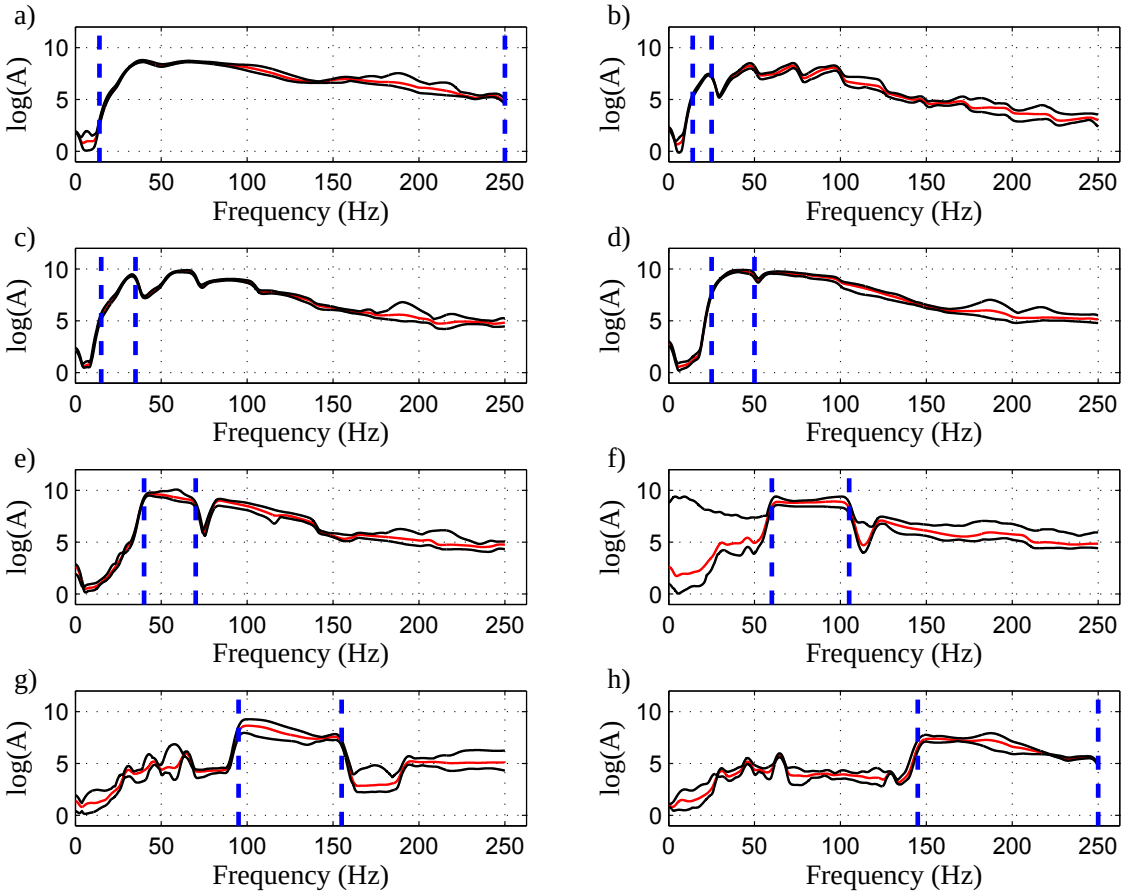

FIG. 2. Source H_1 repeatability comparison. Sweep ranges in Hz are indicated by dashed lines for 14-250 (a) and 14-25 (b). The remainder (c through h) are the same as for V (Figure 1). Lines represent the mean, minuma, and maxima as in Figure 1. Signif cant departure from the mean is seen within and without the target ranges, in particular for sweep 14-250 (a), and for sweeps 60-105 (e) through 145-250 (h).

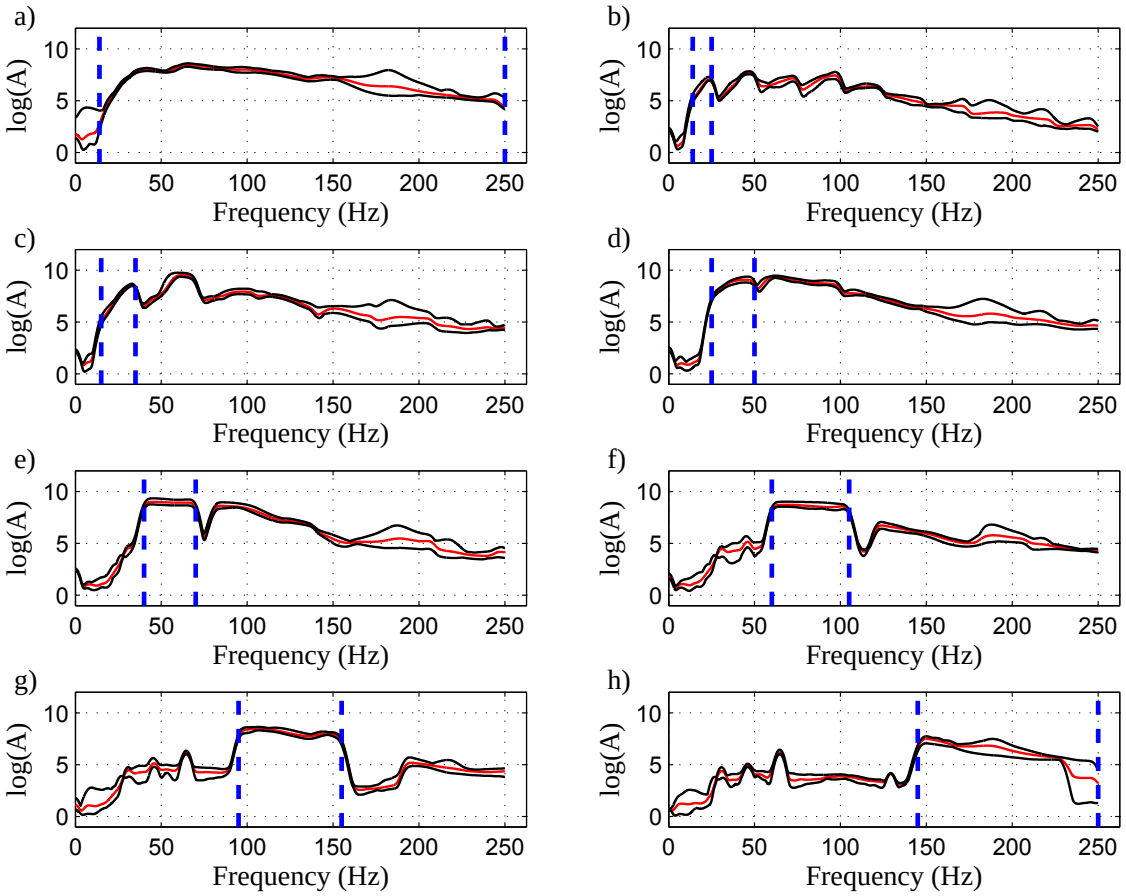

FIG. 3. Source H_2 repeatability comparison. Sweep ranges (indicated by dashed lines) are the same as those for Figure 2. Similarly the red and black lines. Signif cant departure from the mean (red line) is seen within and without all target ranges except 14-25 (b) and 15-35 (c).

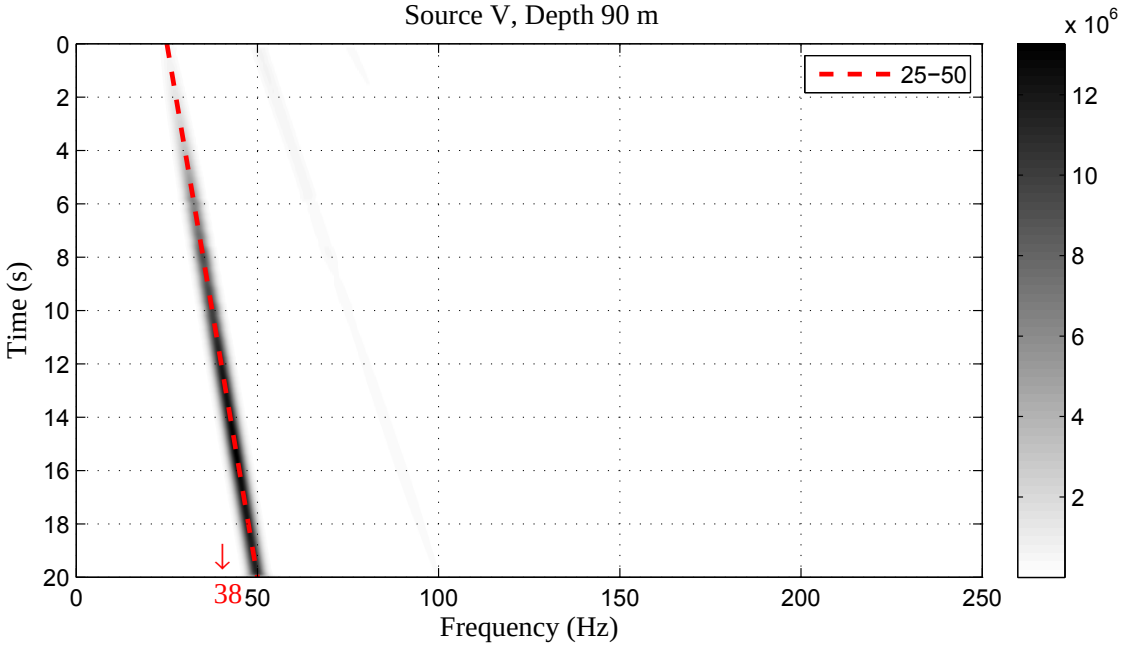

FIG. 4. The vector sum of Gabor power spectra for the surface data corresponding to depth $z = 90$ for the 25-50 Hz sweep from source V. No 38 Hz harmonic is excited.

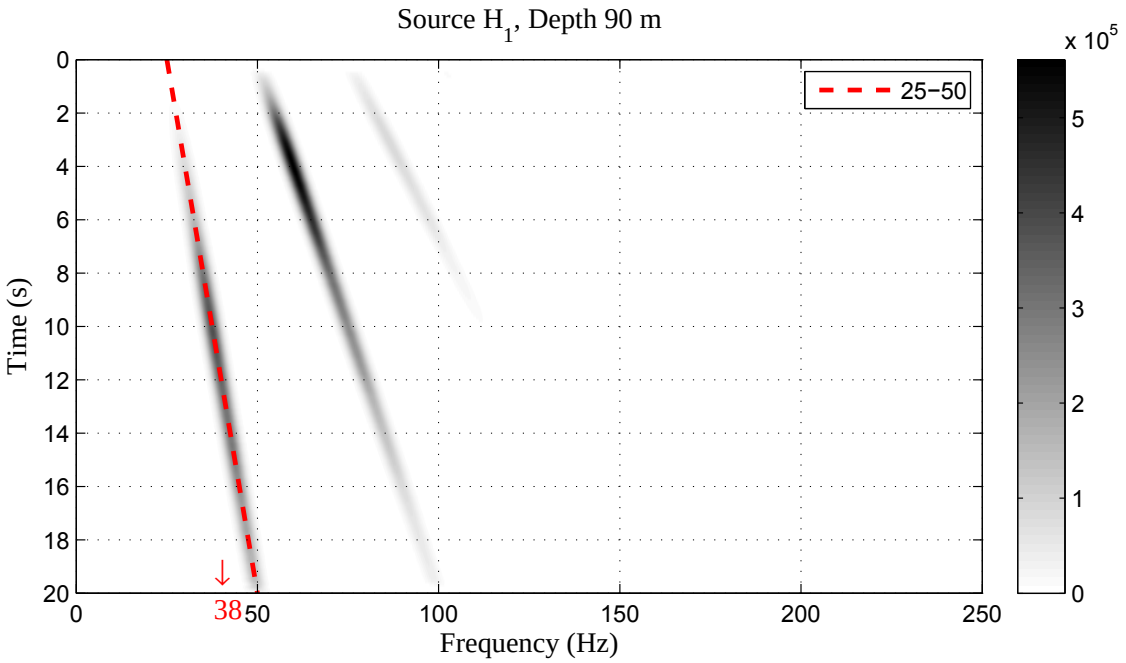

FIG. 5. The vector sum of Gabor power spectra for the surface data corresponding to depth $z = 90$ for the 25-50 Hz sweep from source H_1. No 38 Hz harmonic is excited, and two base-plate harmonics are apparent between 50 and 120 Hz and 0.5 and 20 s.

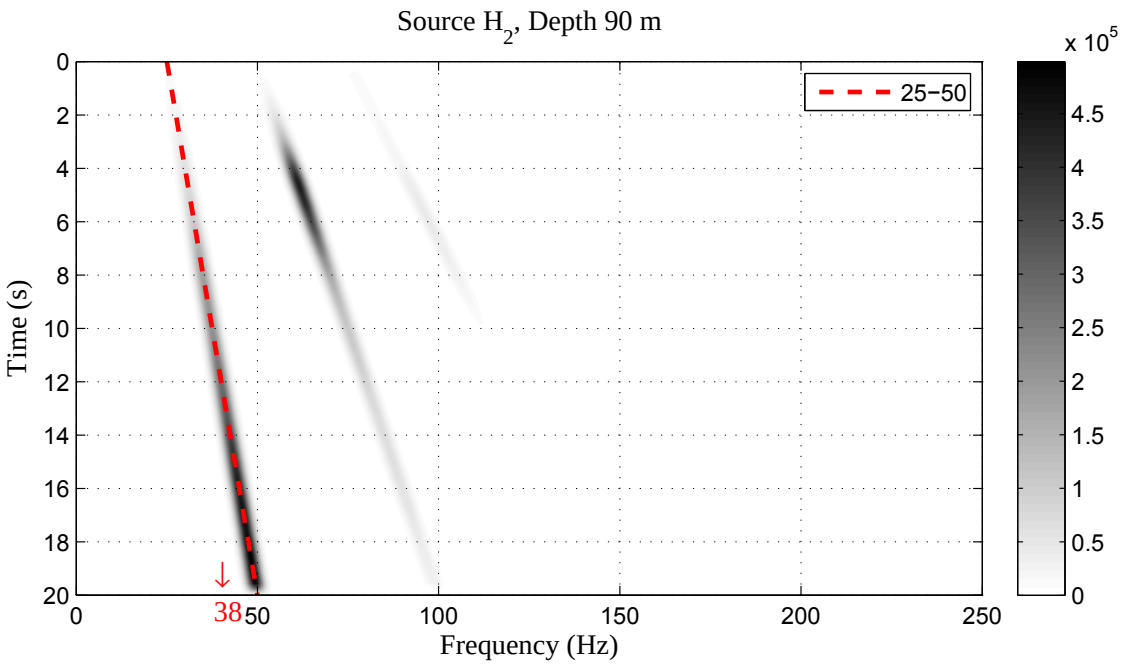

FIG. 6. The vector sum of Gabor power spectra for the surface data corresponding to depth $z = 90$ for the 25-50 Hz sweep from source H_2. No 38 Hz harmonic is excited, and base-plate resonances are apparent.

38 Hz harmonic

An obvious 38 Hz harmonic present on the downhole receiver data. As can bee seen in Figures 7, 8, and 9, this harmonic is strongest for the V source, weaker for H_1, and weakest for H_2. These Gabor spectra correspond to the data from receivers at 90 m in the wellbore, and they are the log-amplitude of a *stack* of three Gabor spectra that correspond to each component of the receiver. For source V, (Figure 7), the harmonic at 38 Hz dominates completely the rest of the sweep energy and harmonics. This harmonic is present for source H_1, but with lesser amplitude; the sweep plus the first harmonic of the sweep are still visible, and noise at 180 Hz is apparent. No harmonic is present for H_2, and the sweep, first harmonic, and noise is present at 60 Hz and at 180 Hz.

The 38 Hz harmonic is absent on the surface data as can be seen on Figures 4, 5, and 6, so it is a manifestation of some property of the well. Further, because it is present only for sources V and H_1, this harmonic is excited by P-, S-, and / or Rayleigh modes, where the S-mode is polarized in the H_1 direction.

Conventional Q analysis requires derivatives in frequency f, and is therefore extremely susceptible to noise sources like harmonics and electrical noise. Equation 5 indicates derivatives only in time τ, so the method presented here is robust in the presence of f-localized noise.

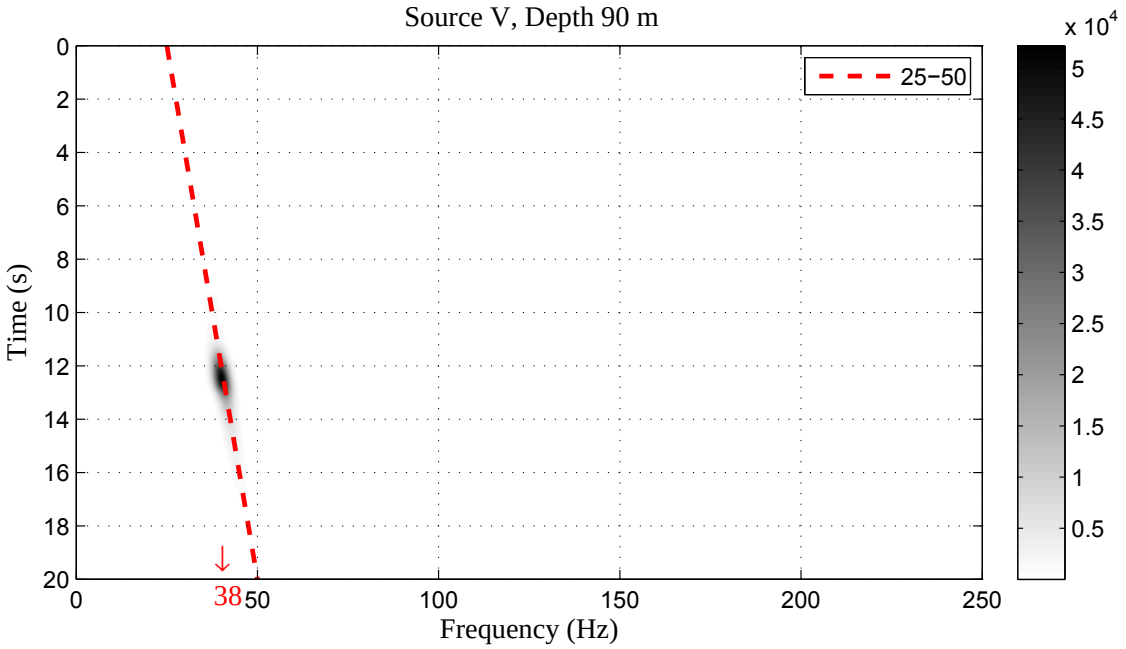

FIG. 7. The vector sum of Gabor power spectra at depth $z = 90$ for the 25-50 Hz sweep from source V. A 38 Hz harmonic is excited.

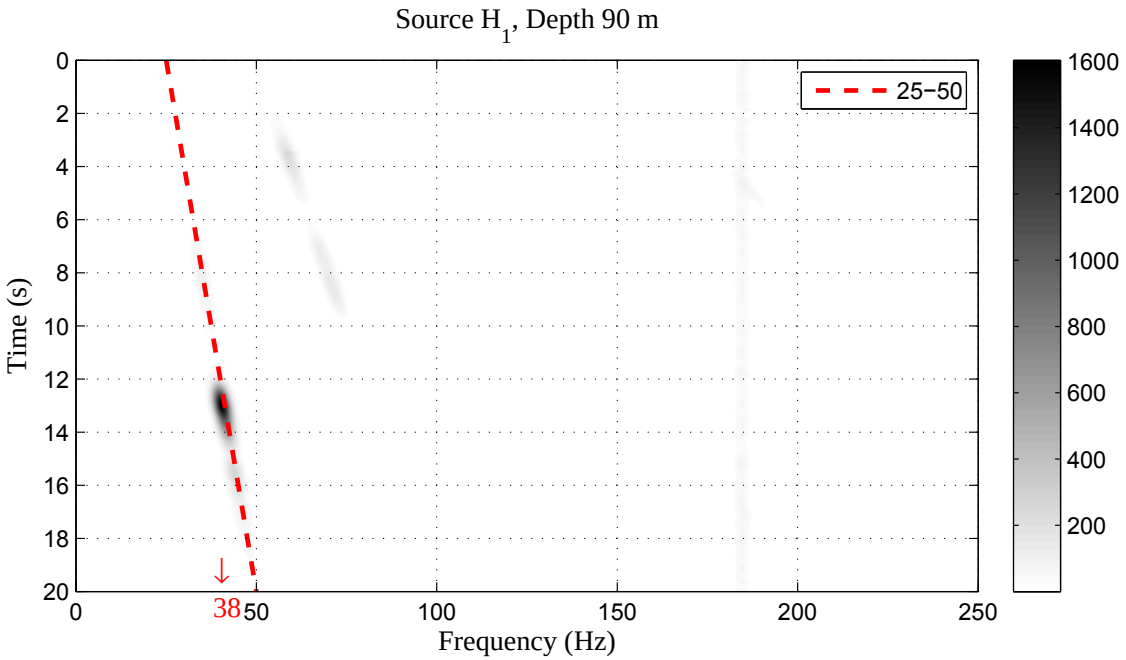

FIG. 8. The vector sum of Gabor power spectra at depth $z = 90$ for the 25-50 Hz sweep from source H_1. A 38 Hz harmonic is excited, but with reduced amplitude relative to source V (Figure 7).

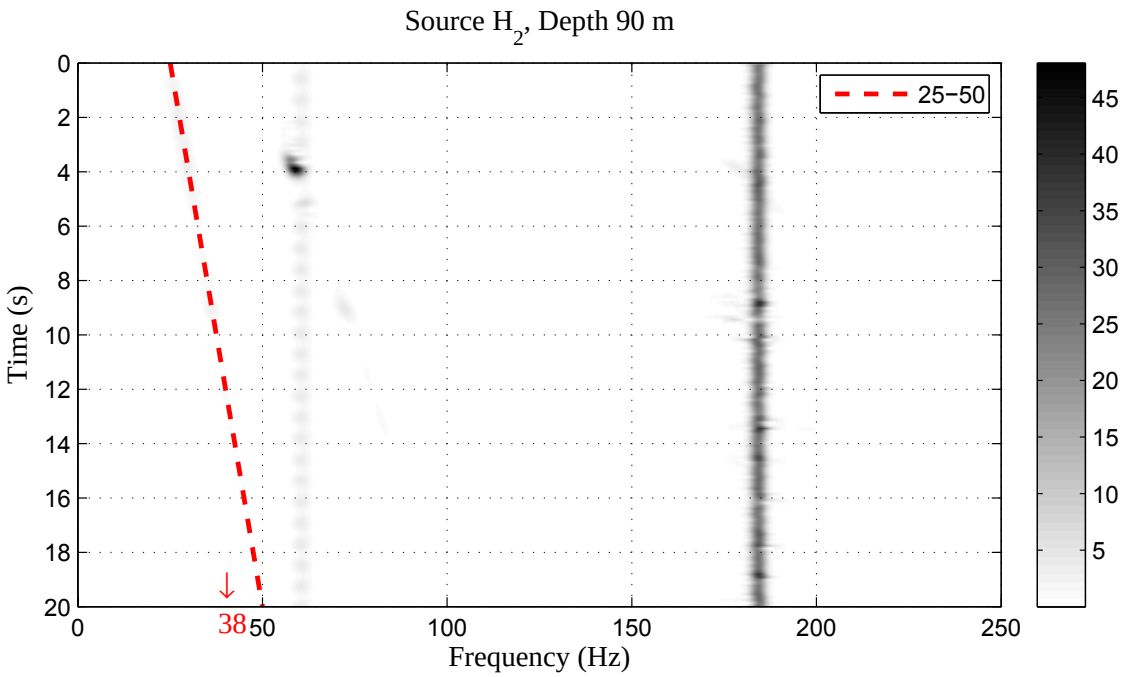

FIG. 9. The vector sum of Gabor power spectra at depth $z = 90$ for the 25-50 Hz sweep from source H_2. The 38 Hz harmonic is not evident, and this recording is dominated by electrical noise.

Rotation analysis

Because data were acquired with a source-wellbore offset of only 10 m, rotation analysis fails to estimate reliable dip ϕ and azimuth θ for the downhole receiver. Here, ϕ (dip) is the angle between a ray defined by the axis of the vertical geophone in the well bore and the angle of incidence of a P-wave to the geophone. Azimuth (θ) is defined as the minimum angle between either of the two horizontal geophones and the plane that contains the wellbore and the source. Estimates of ϕ for each receiver level in the wellbore are deduced based on 3-component analysis of P-wave amplitudes extracted from windowed first-arrivals. Figures 10, 11, and 12 show correlated data for, respectively, source V and sweep 10-250 Hz, source V and sweep 15-35 Hz, and source S_2 and sweep 15-35 Hz. The P-wave first arrival (interpreted) is indicated by a dashed red line. A depth variable P-velocity α is computed from the interpreted line, and it is used to predict S-velocity β using an assumed α/β ratio of 2. The P- and S-wave first arrivals extracted from all 3 components data from source V and source H_2 based on the interpreted first-break times using a short window. Rotation analysis is then done according to Ferguson (2009) to estimate downhole dip ϕ and azimuth θ of each receiver. As can be seen in Figure 13a, analysis fails to converge to a reliable ϕ estimates. For source V, estimates of ϕ based on P-wave amplitudes for each depth level (horizontal axis in Figure 13) and for each of the eight sweeps (Table 1) are indicated by red dots. There are eight red dots per depth level, and the associated scatter indicates significant error. Green dots on Figure 13a indicate ϕ estimates for source H_2 based on S-wave amplitudes. Significant error is suggested also by the scatter of the green dots.

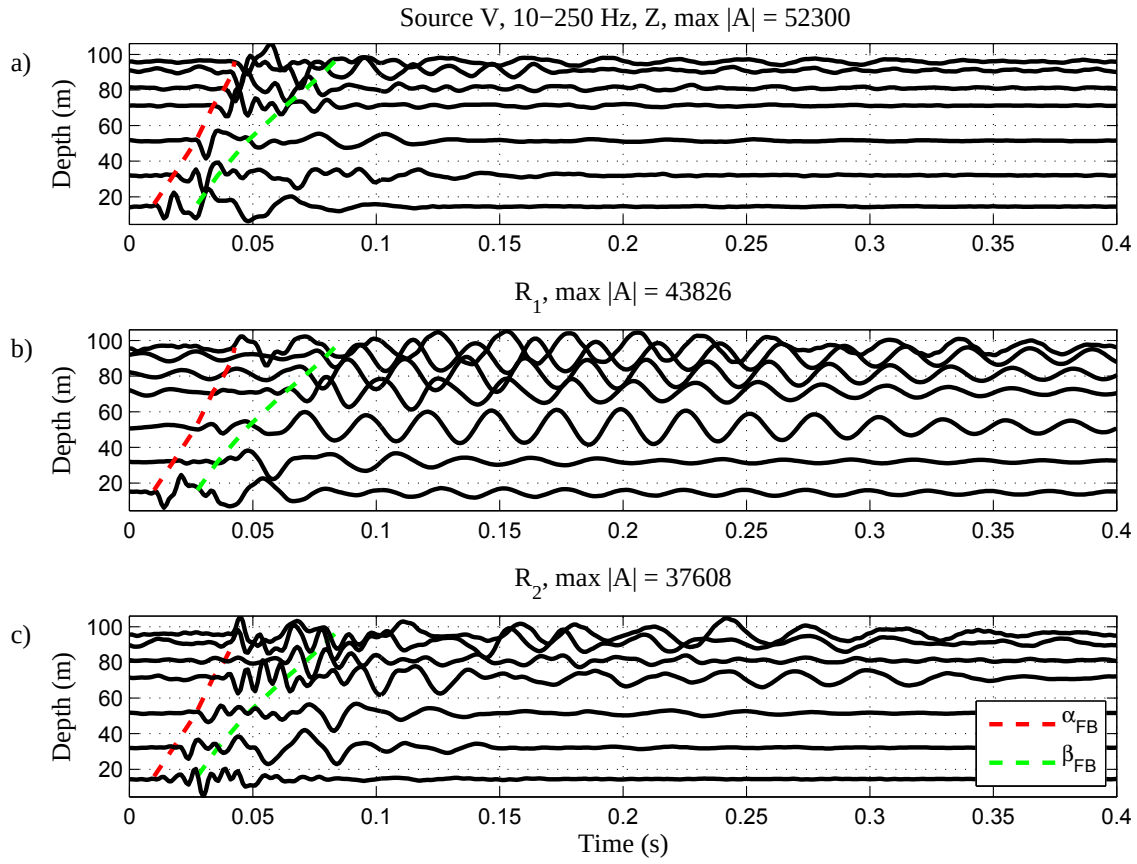

FIG. 10. Correlated data downhole data for source V and sweep 10-250 Hz. P-wave first breaks are indicated by the dashed red line. S-wave first breaks are indicated by the dashed green line. a) Receiver Z. b) Receiver R_1. c) Receiver R_2.

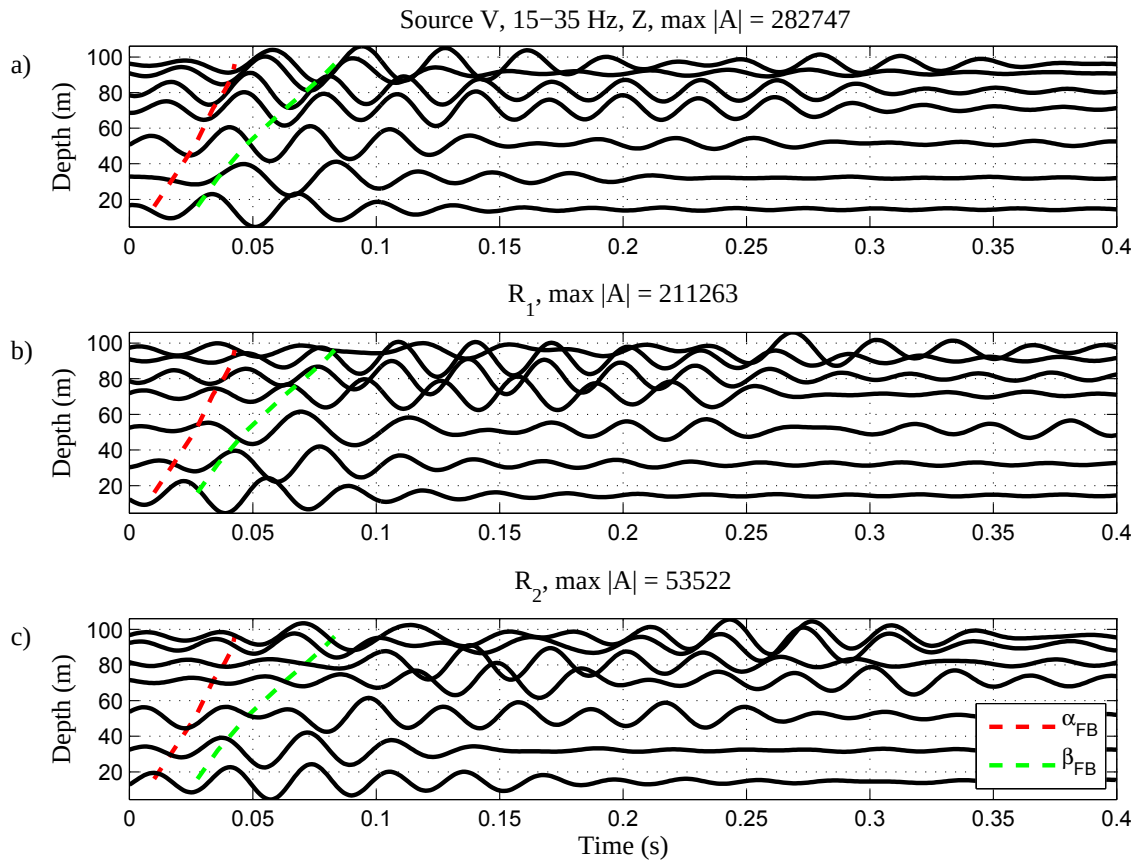

FIG. 11. Correlated data downhole data for source V and sweep 15-35 Hz. a) Receiver Z. b) Receiver R_1. c) Receiver R_2.

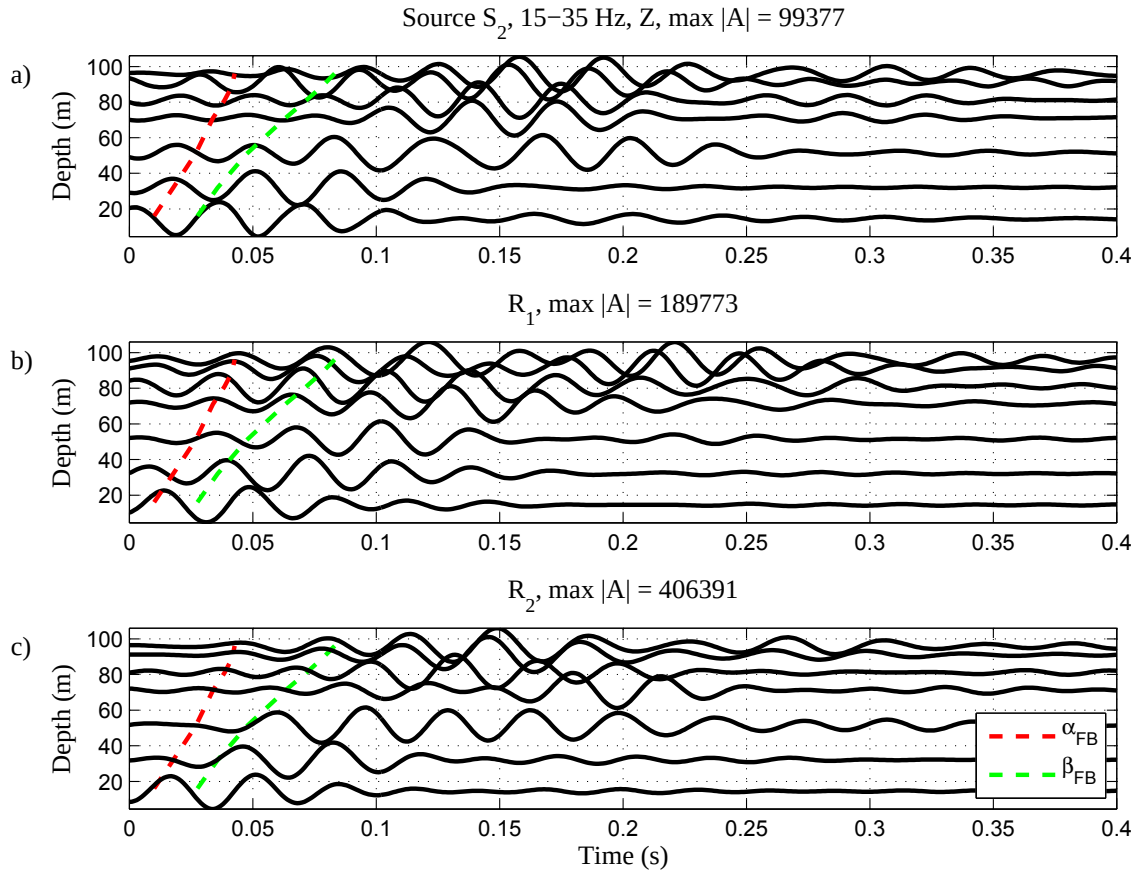

FIG. 12. Correlated data downhole data for source H_2 and sweep 15-35 Hz. a) Receiver Z. b) Receiver R_1. c) Receiver R_2.

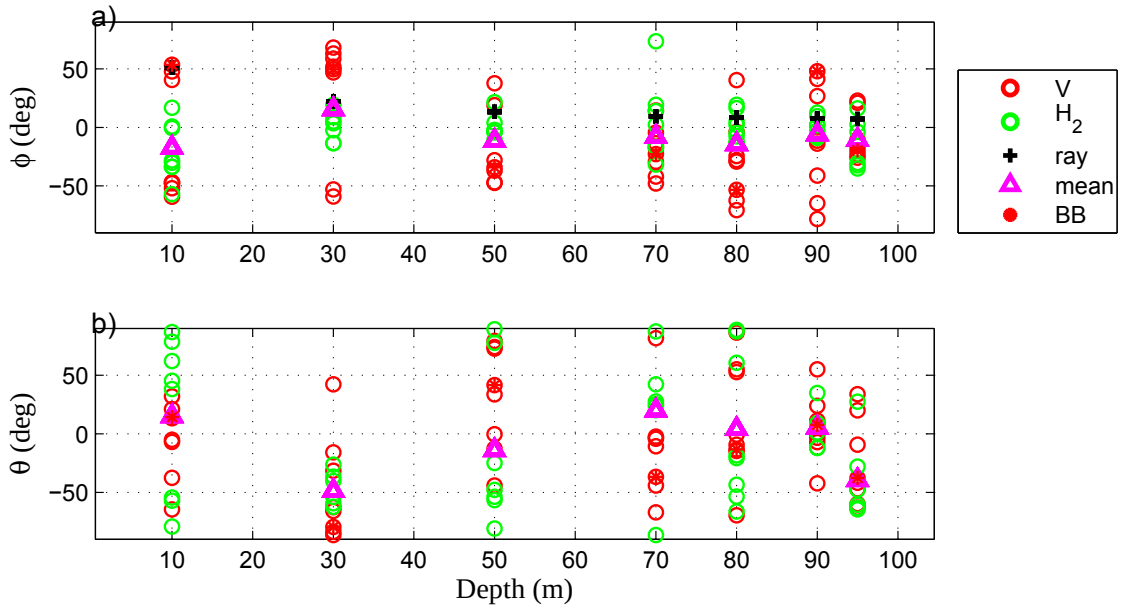

FIG. 13. Rotation analysis. a) Dip estimate. Scatter about the ray-trace estimate (black '+' symbols) indicates signif cant error. b) Azimuth estimate. Signif cant error is present.

Assuming that error $\Delta\phi$ in ϕ is random, the average of all ϕ is computed for each depth level using all ϕ estimates (magenta triangles on Figure 13a). Then, assuming that both the wellbore and component Z are vertical, an estimate of ϕ is make by raytracing from the source location to each depth in turn based on interpreted α. These estimates are plotted as black crosses. With the exception of depth 10 m, the raytrace estimate (black crosses) agrees fairly well with the average from rotation analysis (magenta triangles). Assuming, then, that component Z was vertical in the well, then the average ϕ is about 15 degrees less than the raytraced ϕ for each depth with close agreement at 30 m, and poor agreement at 10 m. It is concluded, then, that there is too much noise, and too little source - wellbore offset to estimate ϕ satisfactorily. Similarly, because of the poor estimates of ϕ, the corresponding estimates of θ (Figure 13b) are assumed to be of little use, again, due to noise and a too-near offset.

DATA PROCESSING

Analysis of the acquired VSP data and surface data uncovers a number of problems as discussed above. Present in the data are source variations between downhole receivers, baseplate harmonics, a 38 Hz harmonic and noise, and poor results from rotation analysis. To mitigate the effects of source variation, the vertical-component surface recordings are used to normalize all downhole recordings in a source / depth consistent way. Then, each uncorrelated VSP component (there are nine components) is corrected for spherical spreading Newman (1973), filtered to within it's sweep range to eliminate baseplate harmonics, and Gabor transformed Sun et al. (2009). Then, because receiver components can not be separated reliably, power spectrum $G\,G^{\dagger}$ is computed for each receiver, and the results are summed into a single spectrum.

For each depth, power spectra for all sweeps are summed as in Figures 14, 15, and 16 for sources V, H_1, and H_2 respectively. Columns in these Gabor matrices quantify the power of one frequency f spread over sweeptime t (distinct from traveltime τ). Because $\beta(f)$ (equation 5) is the result of a scaled τ derivative, overlapping sweeps may be summed along sweep time (vertical axes Figures 14, 15, and 16) as long as sweep overlap is consistent depth-to-depth.

Annotated lines on Figures 14, 15, and 16 indicate expected sweep ranges. All sweeps are present for V. A strong event at $\sim$ 38 Hz is apparent on V and to a lesser extent on H_1 and on H_2, and a baseplate harmonic is apparent on V between 35 and 38 Hz and 0 and 5 s. It also excites amplitudes at 38 Hz. The 38 Hz event is absent on the surface data and is attributed to some property of the well.

Problems associated with H_1 and H_2 result in a number of bad or missing sweeps (Figure 16 indicates sweep 145-250 Hz is missing). Where this occurs, a reference 14-250 Hz sweep is filtered appropriately and scaled (Figure 16 between 10 and 20 s). This replacement does allow leakage of baseplate harmonics that originate in the lower part of the broadband sweep as seen between 0 and 8 seconds. The broadband sweep is otherwise excluded from analysis.

Q ESTIMATION

For each depth and each source, Gabor spectra are integrated along sweep time, then square root and natural logarithm are applied according to equation 5. Frequency curves are plotted as surfaces in Figures 17, 18, and 19. Red dots along τ indicate traveltimes to each receiver. A strong amplitude associated with $\sim$ 38 Hz is apparent on Figure 17 (V). Lesser peaks are associated with 60 Hz, 120 Hz, and 180 Hz. The 38 Hz amplitude is less apparent on the H_2 source data (Figure 19), and the 60 Hz related peaks are very strong. $\log A$ changes abruptly for V, H_1, and H_2 at $\approx$ 0.26 s (≈ 50 m) for all f and coincides with the expected boundary between an upper unit (unsaturated) and a lower unit (groundwater saturated).

Data from Figures 17, 18, and 19 are differentiated along τ (traveltime), and β (RMS) is computed for each f. The resulting $\beta(f)$ are plotted in Figure 20 for each source. Figure 20a indicates effective β for the formation increases with f. Strong noise is present at $\approx$ 38 Hz, and at 60, 120, and 180 Hz (powerline noise). For the upper unit (10-50 m, Figure 20b), β increases strongly with f, and noise is apparent at $\approx$ 38 Hz. Powerline noise is not significant. β is weaker and decreases with f in the lower unit (50-95 m, Figure 20c). The 38 Hz noise is absent, though powerline noise is is very strong.

Linear best-fits (Figure 20, dashed lines) are computed for each $\beta(f)$ (formation, unit 1, unit 2) and inverted for Q according to equation 3. Curves for Q_F (formation), $Q1$ (unit 1), and $Q2$ (unit 2) are plotted against f in Figure 21, and effective Q_e for the formation is computed according to

$$1/Q_e = [\tau_1/Q_1 + \tau_2/Q_2]/\tau, \tag{6}$$

where τ_1, and τ_2 are traveltimes in units 1 and 2, and $\tau = \tau_1 + \tau_2$ (Båth, 1974; Dasgupta and Clark, 1998). Q estimates all increase with f until about 100 Hz and then rise exponentially

(not shown) and indicate, perhaps, the usable f range. Calculated Q_e (Figure 21, dashed line) does not lie close to Q_F (Figure 21, red line).

DISCUSSION AND CONCLUSIONS

We use the Gabor domain to identify noise sources and verify sweep fidelity, and most importantly, we use it to estimate Q based on traveltimes of monochromatic wavefields in the subsurface. Our use of long, narrowband sweeps, reduces noise effects due to baseplate harmonics.

We identify a possible indicator for the transition from unsaturated to water saturated on our plots of $\log A(\tau, f)$ at $\approx$ 50 m[†]. From the $\log A$ data, we deduce attenuation β curves for the formation, and curves for the saturated (weak β, decreases with f) and unsaturated (strong β, increases with f) units. Due to significant noise still present in the data, and because of the small number of depths sampled, Q for the formation and units is estimated with β best-fits. Q values for the formation and both units increase with f below 100 Hz beyond which they rise exponentially. Measured Q for the formation and effective Q (calculated) are not in close agreement, so doubt is cast on all of the Q estimates. We anticipate that a 10-fold increase in the number of depth levels acquired, and greater attention to noise reduction in the field will improve Q estimates.

ACKNOWLEDGEMENTS

The author wishes to thank the sponsors, faculty, and staff of the Consortium for Research in Elastic Wave Exploration Seismology (CREWES), and the Natural Sciences and Engineering Research Council of Canada (NSERC, CRDPJ 379744-08) for their support of this work.

REFERENCES

Båth, M., 1974, Spectral analysis in geophysics, *in* Developments in solid earth geophysics, Elsevier Scientific Publishing Company, Amsterdam.

Dasgupta, R. and R. A. Clark, 1998, Estimation of Q from surface seismic reflection data: Geophysics, **63**, 2120–2128.

Ferguson, R. J., 2009, Geophone rotation analysis by polarity inversion: CREWES Research Report, **21**.

Jannsen, D., J. Voss, and F. Theilen, 1985, Comparison of methods to determine Q in shallow marine sediments from vertical reflection seismograms: Geophys. Prosp., **33**, 479–497.

Newman, P., 1973, Divergence effects in a layered earth: Geophysics, **38**, 481–488.

Sun, L. F., B. Milkereit, and D. R. Schmitt, 2009, Measuring velocity dispersion and attenuation in the exploration seismic frequency band: Geophysics, **74**, WA113–WA122.

Toverud, T. and B. Ursin, 2005, Comparison of seismic attenuation models using zero-offset vertical seismic profiling (vsp) data: Geophysics, **70**, F17–F25.

Zener, C. M., 1948, Elasticity and anelasticity of metals: University of Chicago Press.

[†]A watertable depth of 50 m is consistent with field observations.

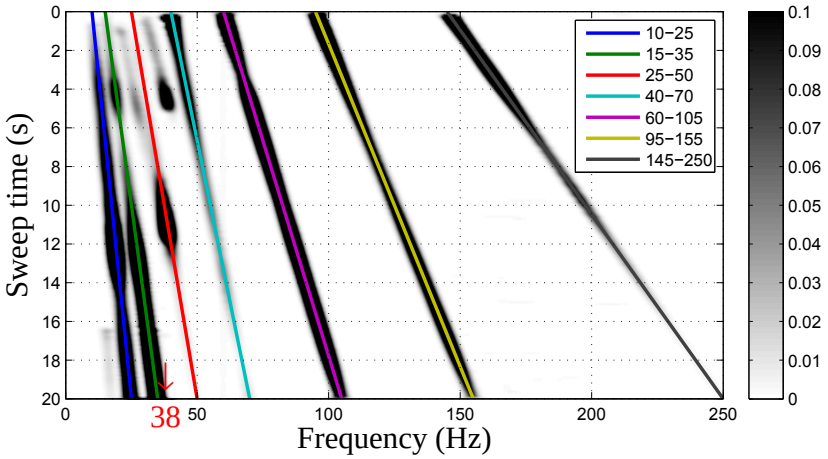

FIG. 14. Source V Gabor power spectra for $z = 50$ m.

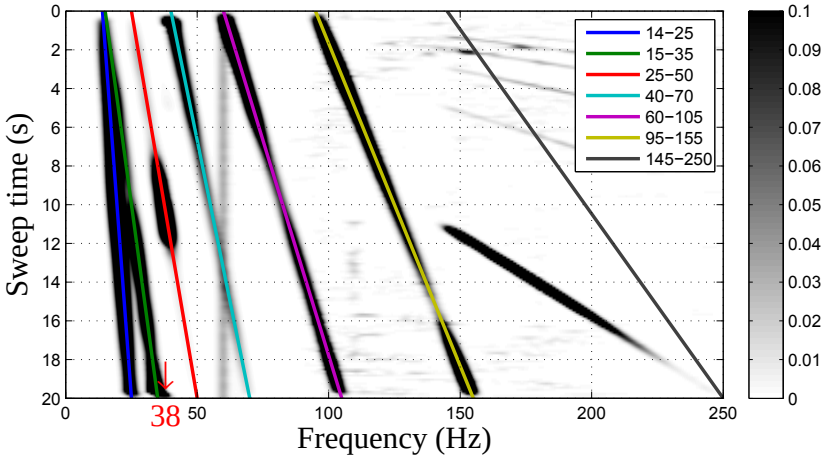

FIG. 15. Source H_1 Gabor power spectra for $z = 50$ m.

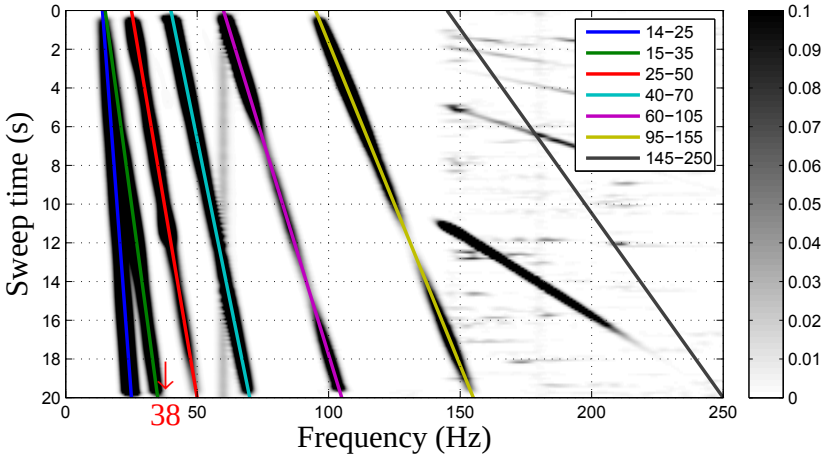

FIG. 16. Source H_2 Gabor power spectra for $z = 50$ m.

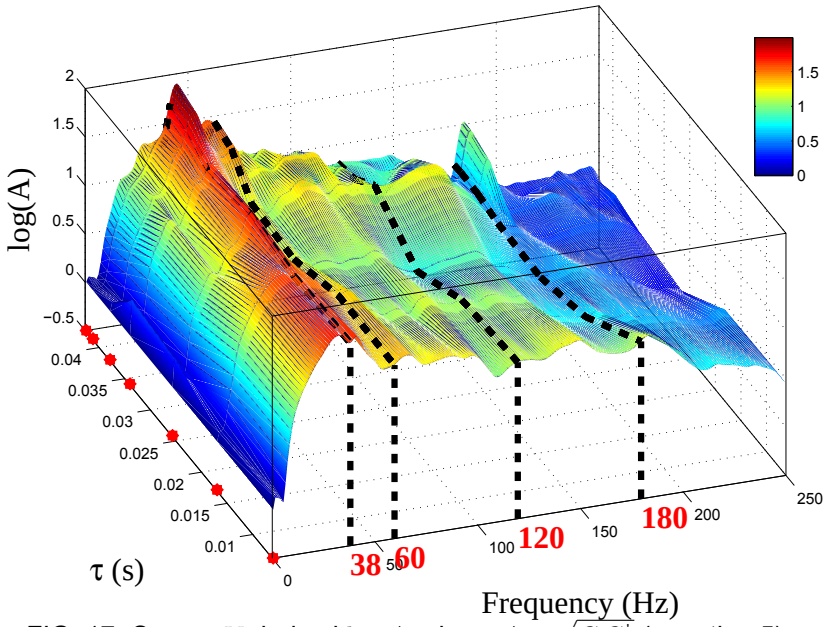

FIG. 17. Source V derived $\log A$, where $A = \sqrt{G\,G^{\dagger}}$ (equation 5).

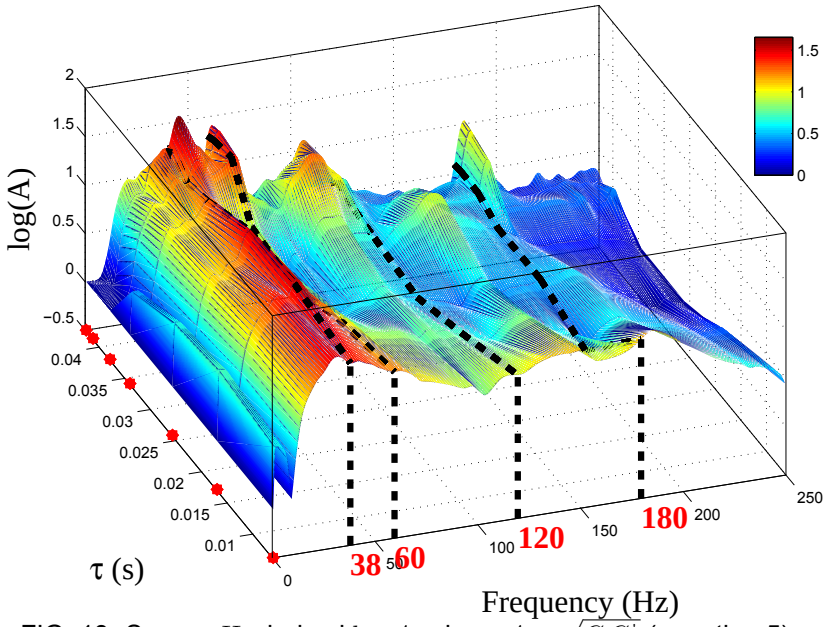

FIG. 18. Source H_1 derived $\log A$, where $A = \sqrt{G\,G^{\dagger}}$ (equation 5).

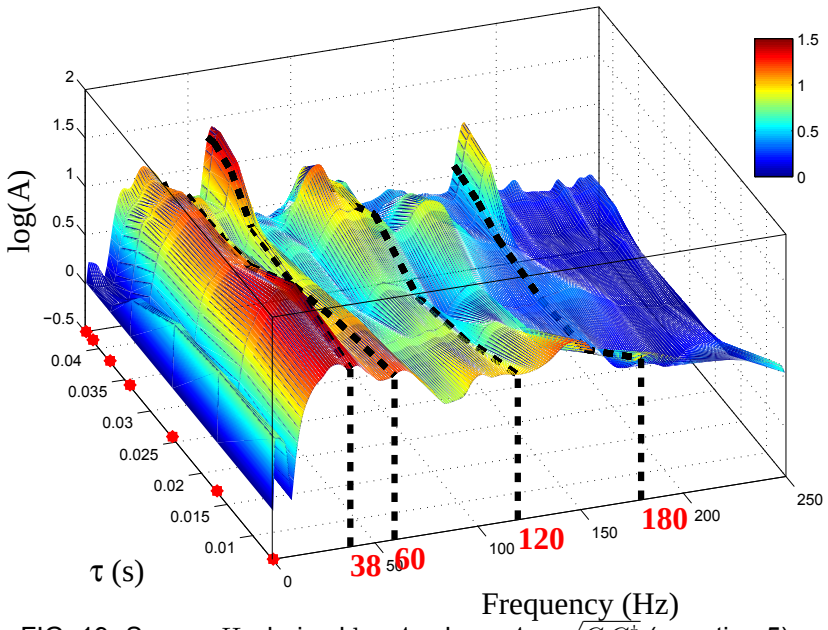

FIG. 19. Source H_2 derived $\log A$, where $A = \sqrt{G\,G^{\dagger}}$ (equation 5).

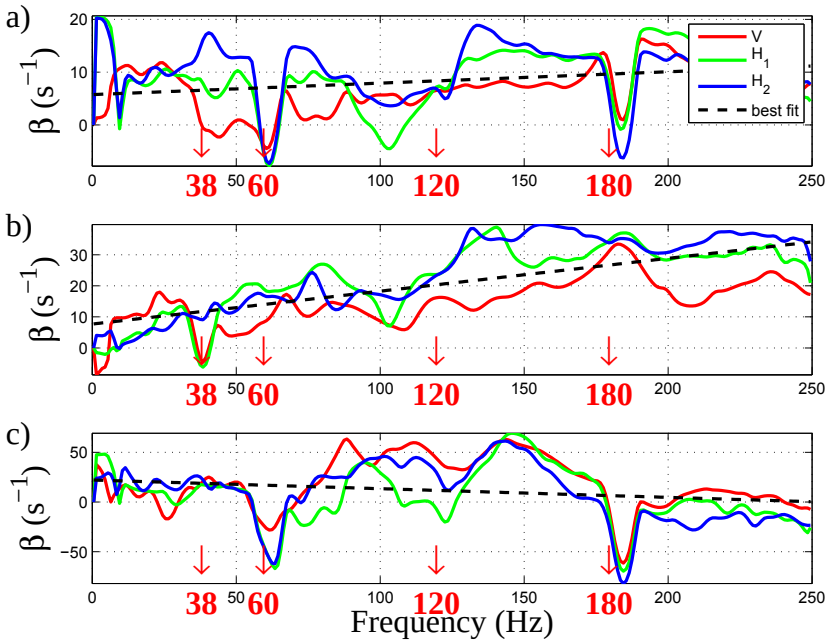

FIG. 20. Attenuation β. a) Depths 10-95 m. b) Depths 10-50 m. c) Depths 70-95 m.

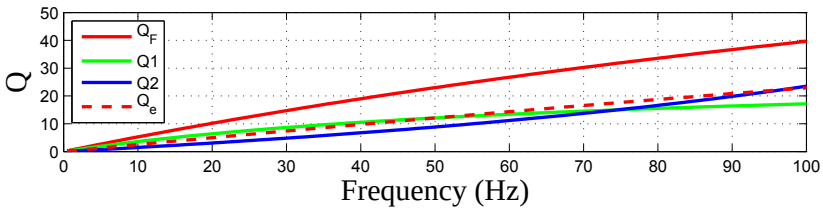

FIG. 21. $\mathrm{Q}(f)$. a) Depths 10-95 m. b) Depths 10-50 m. c) Depths 50-95 m.